LETTERS
PUBLISHED ONLINE: 24 NOVEMBER 2014 | DOI: 10.1038/NGEO2300
nature geoscience

Large-scale variations in the stoichiometry of marine organic matter respiration

Tim DeVries[1,2*†] and Curtis Deutsch[3]

The elemental composition of marine organic matter governs resource competition among plankton, and couples the global cycles of carbon, nutrients and oxygen. Observations have revealed systematic large-scale variation in the ratios of these essential elements removed from surface waters by phytoplankton[1–5]. However, an impact of this variability on deep ocean properties has not been detected. Here we use a data-constrained ocean circulation model and observed long-term mean distributions of dissolved oxygen and the nutrient phosphate to show that there is a threefold variation across latitudes in the amount of dissolved oxygen consumed per unit of phosphate released during organic matter respiration. This pattern of remineralization ratios is shown to significantly modify the extent and distribution of low-oxygen water masses in the interior ocean. We also find that ocean biomes with distinct light and nutrient availability are characterized by different regional stoichiometries. These findings suggest that in a more stratified ocean, an increase in light exposure and decrease in nutrient concentration could raise the C:P ratio of phytoplankton, and the associated carbon storage by the ocean's biological pump.

The elemental ratios of plankton biomass are of fundamental importance in oceanography. They are used to infer the limiting nutrient for phytoplankton growth[6], to predict the sensitivity of ocean carbon storage to climate change[7], and to understand how distinct elemental cycles are linked over geologic time[8]. The mean stoichiometry of plankton biomass is closely matched by the correlations among nutrients and oxygen in the deep ocean[9]. Empirical analyses and numerical models of carbon and nutrient cycling thus commonly assume uniform stoichiometric ratios for organic matter production and respiration[10]. Stoichiometric differences within and between plankton species are widely recognized, however, and recent studies have found that organic matter formed in the sunlit surface ocean exhibits widely varying proportions of carbon and nutrients[1–5]. Such large-scale differences in ecosystem stoichiometry may have important consequences for the deep ocean[11], but their signals have not been directly detected from observations.

Persistent and large-scale variations in organic matter stoichiometry should be reflected in the sub-surface distributions of dissolved inorganic carbon, oxygen and nutrients. Detecting these signals is complicated by the fact that ocean circulation can transport substantial concentrations of each constituent from the surface to depth. These 'preformed' concentrations[9] do not result from organic matter remineralization, and must be subtracted from observed concentrations to determine the nutrients released and oxygen consumed by organic matter decomposition, which are termed 'regenerated'. Such corrections require an accurate depiction of how surface waters are mapped via the circulation into the interior ocean. Early analyses of regenerated ratios only coarsely accounted for the contribution of a few surface water types, yielding ratios averaged over whole ocean basins[12–14].

Here, we use a data-constrained ocean circulation model[15,16], along with global observations of phosphate[17] (PO_4^{3-}) and dissolved oxygen[18,19] (O_2) concentrations, to separate sub-surface oxygen and phosphate pools into their preformed and regenerated components (Methods), at a resolution that permits detection of regional variations in organic matter stoichiometry. Because most of the oxygen consumed during organic matter decomposition is used in the oxidation of organic carbon, the ratio of O_2 consumed to PO_4^{3-} released is closely related to the C:P ratio of organic carbon, but lacks the complicating factor of anthropogenic CO_2 uptake[14]. We analyse phosphate rather than nitrate, because plankton C:N ratios are generally less variable than C:P ratios[20] and the nitrate distribution is influenced by processes such as denitrification, in addition to organic matter stoichiometry.

Our analysis yields a O_2:P regeneration ratio, $R_{O_2:P}$ (Methods; equation (1)), with a global mean value of ∼150:1, in line with previous studies[21]. However, the distribution of $R_{O_2:P}$ exhibits large and spatially coherent deviations from the mean value. Below the euphotic zone at 200 m depth, the gradients in $R_{O_2:P}$ are predominantly latitudinal and hold in all ocean basins (Fig. 1a,b). Highest $R_{O_2:P}$ values of >200:1 occur in the subtropical gyres and Antarctic waters, whereas the lowest $R_{O_2:P}$ values of ∼60:1 occur in the sub-Antarctic, North Pacific and North Atlantic. The $R_{O_2:P}$ in equatorial regions is generally close to the mean ocean value of ∼150:1 (Fig. 1a,b). The latitudinal and inter-basin patterns are also coherent throughout the water column, although the magnitude of variation decreases rapidly with depth (Fig. 1c). In the deep ocean respiration rates are weaker, and the ocean circulation more effectively homogenizes regenerated nutrient and oxygen concentrations[3]. The vertical extent of the $R_{O_2:P}$ signal is greatest in the high latitudes, where waters circulate along density surfaces to greater depths (Fig. 1c).

These patterns are robust to uncertainties in the compensation depth (the depth below which respiration rates exceed photosynthesis rates), the depth of the surface mixed layer, the seasonal variation of oxygen and nutrient concentrations, and uncertainties in ocean circulation (Fig. 1a; see also Supplementary Fig. 1). Sensitivity to the compensation depth is greatest in subtropical regions, where deeper compensation depths imply higher sub-surface $R_{O_2:P}$ values. Because subtropical gyres have deep euphotic zones owing to a lack of chlorophyll and associated light-absorbing pigments, the $R_{O_2:P}$ in these regions is probably near

[1]Department of Atmospheric and Oceanic Sciences, University of California, Los Angeles, California 90095, USA. [2]Earth Research Institute, University of California, Santa Barbara, California 93106, USA. [3]School of Oceanography, University of Washington, Seattle, Washington 98195, USA.
[†]Present address: Department of Geography, University of California, Santa Barbara, California 93106, USA. *e-mail: tdevries@geog.ucsb.edu

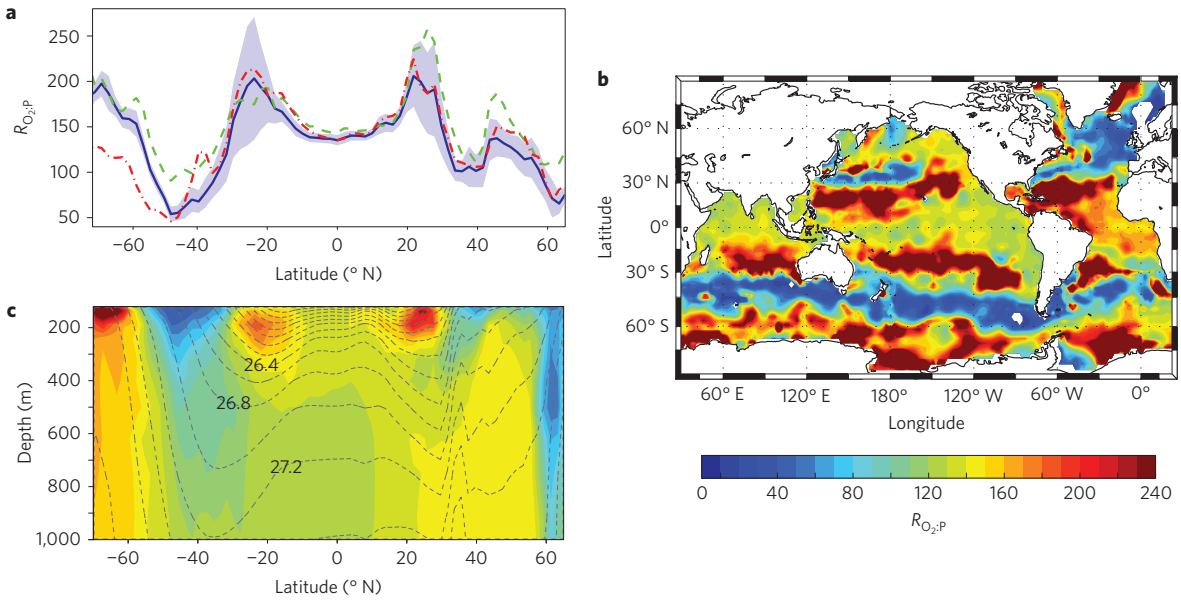

Figure 1 | O_2:P regeneration ratios in the sub-surface ocean. a, Solid blue curve: ensemble mean of the zonal median $R_{O_2:P}$ at 200 m depth diagnosed from a data-constrained ocean circulation model and annually averaged O_2 and PO_4^{3-} observations. Shading: 1σ uncertainty due to ocean circulation and compensation depth. Dot-dashed red curve: as solid curve, but from a model without a surface mixed layer. Dashed green curve: as solid curve, but using winter-averaged tracer observations. **b**, The ensemble median $R_{O_2:P}$ at 200 m diagnosed from annually averaged observations. White regions: excluded from analysis. **c**, The ensemble mean of the zonal median sub-surface $R_{O_2:P}$ diagnosed from annually averaged observations. Same colour scale as **b**. Dashed contours: potential density (σ_θ: contour interval 0.2 kg m^{-3}).

the upper end of the estimated uncertainty (Fig. 1a). Uncertainty in sub-surface $R_{O_2:P}$ due to seasonality of surface O_2 and PO_4^{3-} concentrations is greatest in the high latitudes, particularly in the sub-Antarctic region. Using winter-averaged O_2 and PO_4^{3-} concentrations, which may better represent preformed properties because most deep mixing occurs in winter months, results in higher sub-surface $R_{O_2:P}$ values (Fig. 1a). Sensitivity to circulation, in particular the depth of the surface mixed layer, is greatest in the Antarctic region where shallower surface mixed layers result in lower sub-surface $R_{O_2:P}$ values (Fig. 1a).

The detection of these signals at depths below the euphotic zone provides a view of the stoichiometry of total organic matter export, including both particulate and dissolved organic matter[22]. Moreover, these tracer signals integrate the products of exported organic matter over years or longer (Supplementary Fig. 2), implying that the patterns are persistent over time. The latitudinal variation in $R_{O_2:P}$ in sub-surface waters are broadly consistent with measurements of the C:P ratio of surface particulate organic matter[4]. This suggests that $R_{O_2:P}$ primarily reflects variations in C:P ratios of organic matter formed in the surface ocean, and exported to depth via sinking particles. Given the relatively dense coverage of tracer data, our results also confirm that the stoichiometric patterns inferred from sparse measurements of short-lived particulate matter are representative of global patterns. The latitudinal trend in $R_{O_2:P}$ from our analysis differs from the observed trend in particulate C:P ratios[4] only in the Antarctic region, where relatively sparse observations indicate that $R_{O_2:P}$ is higher than average but particulate C:P ratios are not. The apparent discrepancy between surface particle C:P ratios and the $R_{O_2:P}$ of underlying waters, if substantiated by more direct observations, could imply a higher oxidation state of organic C in the polar ocean, for example due to an elevated hydrogen content[10].

The spatial pattern in sub-surface $R_{O_2:P}$ coincides with regional differences in the key parameters governing planktonic growth. We calculated the mean $R_{O_2:P}$ at 200 m depth in 13 different oceanic regions defined by their surface light and nutrient levels averaged over the mixed layer, and by the presence of seasonal sea ice (Fig. 2). The highest $R_{O_2:P}$ values occur below regions of high-light levels and low-nutrient concentrations (L^+N^-), whereas lowest $R_{O_2:P}$ values occur below low-light and high-nutrient (L^-N^+) regions. The L^+N^- areas of the subtropical gyres have the highest sub-surface $R_{O_2:P}$ values in all ocean basins, with the exception of the South Atlantic (Fig. 2b). Lowest $R_{O_2:P}$ values occur in the L^-N^+ areas of the North Atlantic and the Southern Ocean north of the seasonal sea-ice zone. In regions of intermediate surface light and nutrient levels, sub-surface $R_{O_2:P}$ also generally exhibits intermediate values, with some significant inter-basin differences (Fig. 2b). Some of these are upwelling regions, where waters at 200 m are old enough (>50 years, see Supplementary Fig. 2) to have accumulated the products of remineralization from surface waters of both high and low C:P ratios. In these regions, including the sub-Arctic Pacific, the Antarctic, and the equatorial Indian and Pacific oceans, the sub-surface $R_{O_2:P}$ value is less likely to match the stoichiometry of local surface organic matter export. Seasonal sea-ice zones are characterized by relatively high $R_{O_2:P}$, which could reflect the influence of high-light levels due to shallow mixed layers and long day lengths during the summer growing season (Fig. 2).

The correlations between $R_{O_2:P}$ and the surface light and nutrient environment are consistent with plankton C:P variability predicted by resource allocation models[23,24], and with culture studies[20] and direct manipulations of phytoplankton populations[25]. Taxonomic differences could also explain some of the strong gradients in sub-surface $R_{O_2:P}$ inferred here. For example, diatoms tend to dominate high-latitude ecosystems, which could partly explain the trend to lower $R_{O_2:P}$ (and presumably C:P) values in these regions[2,3]. Disentangling the roles of taxonomic and environmental effects on organic matter stoichiometry is not possible from our analysis, but is an important task for developing accurate models of ocean biogeochemistry.

Large-scale variations in $R_{O_2:P}$ have important implications for the distribution of low-O_2 waters in the interior ocean. These effects can be evaluated by multiplying the regenerated PO_4^{3-} distribution by the global mean $R_{O_2:P}$. This yields an O_2 distribution that would occur in an ocean with a constant stoichiometry,

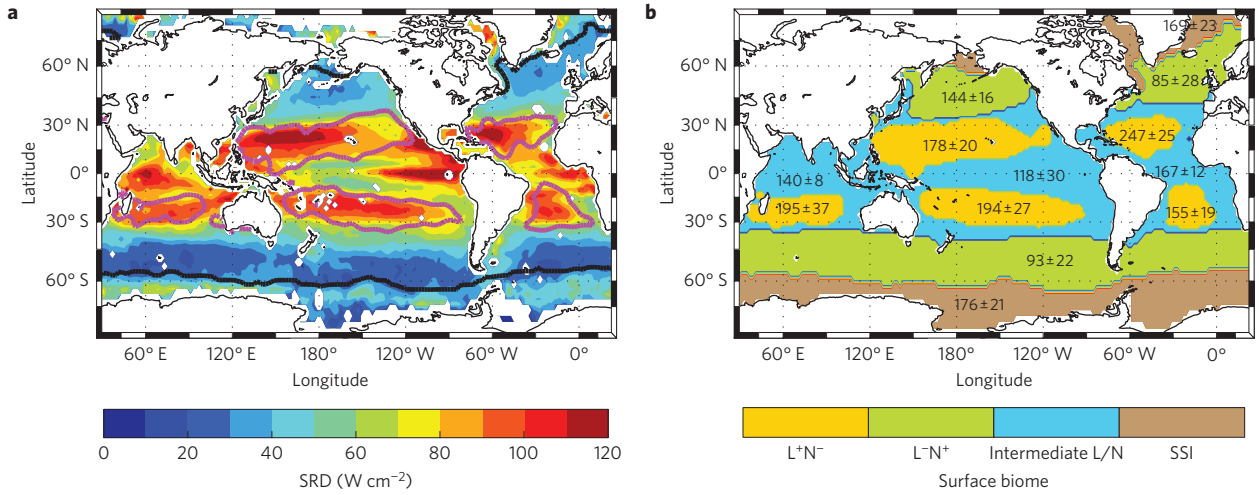

Figure 2 | Surface biomes and sub-surface O_2:P regeneration ratios. a, Chlorophyll-weighted and mixed layer-averaged annual solar radiation dose (SRD, W cm^{-2}, colour scale; see Supplementary Methods). Also shown are low-nutrient regions (annually averaged surface $NO_3^- < 0.3\,\mu M$, thick magenta lines), and maximum seasonal sea-ice extent (thick black lines). **b**, The mean ($\pm 1\sigma$) of the ensemble median $R_{O_2:P}$ at 200 m depth within 13 regions defined by their environmental conditions: high-light low-nutrient regions (L^+N^-, $NO_3^- < 0.3\,\mu M$ and SRD > 80 W cm^{-2}, yellow shading); low-light high-nutrient regions (L^-N^+, $NO_3^- > 3\,\mu M$ and SRD < 50 W cm^{-2}, green shading); regions experiencing intermediate light or nutrient levels (light blue shading); and regions affected by seasonal sea ice (SSI, brown shading).

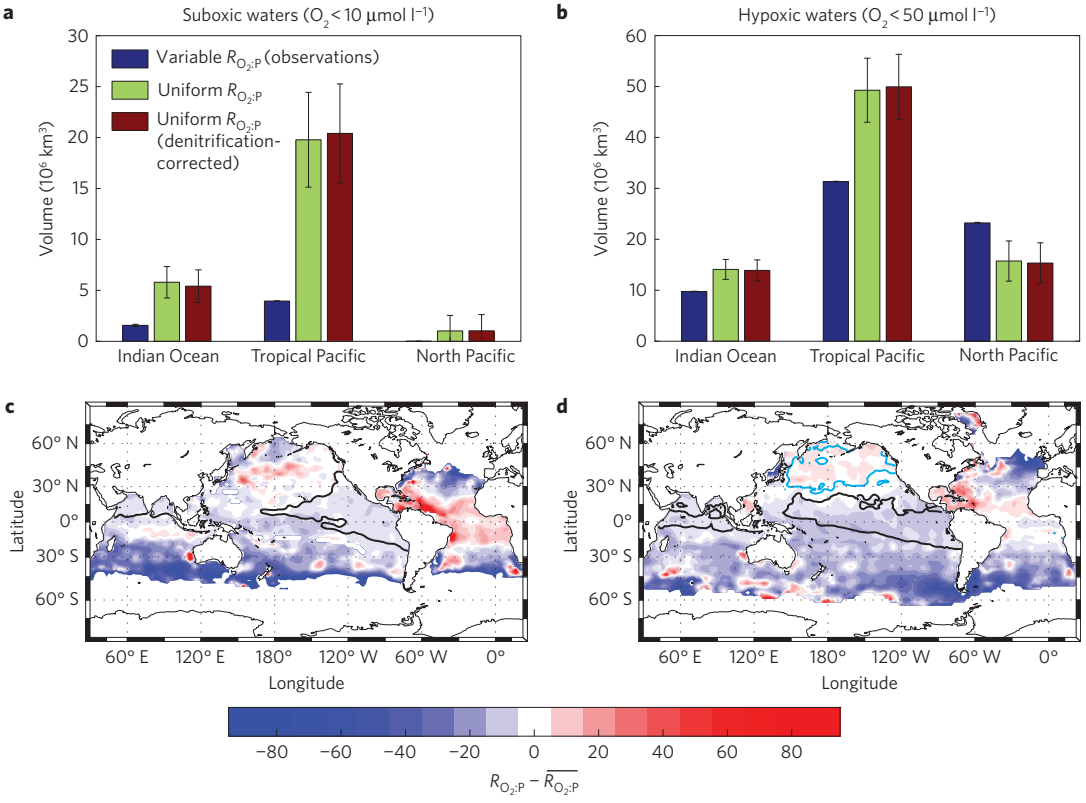

Figure 3 | Impact of variable stoichiometry on low-oxygen waters. a, Volume of suboxic water ($O_2 < 10\,\mu mol\,l^{-1}$) calculated from observations, and as predicted under uniform $R_{O_2:P}$, with and without correcting for denitrification. Error bars: 1-σ uncertainty from ensemble of simulations. **b**, As in **a**, but for hypoxic waters ($O_2 < 50\,\mu mol\,l^{-1}$). **c**, Difference between local $R_{O_2:P}$ (denitrification-corrected) and global average $R_{O_2:P}$ ($\overline{R_{O_2:P}}$) for potential density $26.6 < \sigma_\theta < 26.9$, characteristic of suboxic waters. Black curve marks area in which the difference between the thickness of uniform $R_{O_2:P}$-predicted and observed suboxic waters is >200 m. **d**, As **c**, but for $26.9 < \sigma_\theta < 27.3$, characteristic of hypoxic waters. Light blue curve marks the area in which the uniform $R_{O_2:P}$-predicted thickness bias is <−200 m.

assuming no change in the distribution of regenerated PO_4^{3-} (see Methods and Supplementary Methods). In an ocean with uniform organic matter stoichiometry, the volume of suboxic waters favouring anaerobic microbes ($O_2 < 10\,\mu mol\,l^{-1}$) is nearly five times greater than observed, both globally and in the Tropical Pacific (Fig. 3a). The extent of hypoxic waters stressful to macrofauna ($O_2 < 50\,\mu mol\,l^{-1}$) predicted under uniform stoichiometry is larger than observed in the Indian Ocean and the Tropical Pacific,

but is significantly smaller than observed in the North Pacific (Fig. 3b). These biases can be traced back to spatial variation in O_2:P regeneration ratios. Low-oxygen waters of the Tropical Pacific and Indian oceans exhibit lower $R_{O_2:P}$ than the global average, both in suboxic and hypoxic regions (Fig. 3c,d). Assuming a uniform O_2:P regeneration ratio therefore overestimates net oxygen consumption in these regions. On the other hand, hypoxic waters in the North Pacific experience higher-than-average $R_{O_2:P}$ (Fig. 3d), so that assuming a uniform O_2:P regeneration ratio underestimates O_2 consumption there. Similar biases are almost universally expressed in state-of-the-art Earth System Models with uniform C:P stoichiometry[26], underscoring the importance of including spatial variations of plankton stoichiometry in climate model projections of ocean hypoxia.

Regional differences in the stoichiometry of organic matter export may also alter the sensitivity of the ocean carbon cycle to climate change. As the oceans warm and become more stratified, larger areas are predicted to become relatively depleted of surface nutrients, a condition that is associated with high C:P ratios in the contemporary ocean. A reduction in the depth of the surface mixed layer will also increase the average light levels experienced by phytoplankton. If this occurs during the growing season, it could further elevate the C:P ratios of plankton, especially in areas such as the sub-Antarctic, where light limitation at present seems to reduce plankton C:P ratios. Shifts towards plankton growth with a higher carbon to nutrient ratio in these areas would increase the carbon storage relative to an ocean with fixed stoichiometry. Together these effects could constitute a negative feedback on atmospheric CO_2 increase which is at present lacking in Earth System Models with a fixed stoichiometry[27,28].

Methods

Here we summarize the methods used in this study. Further details can be found in the Supplementary Methods.

Preformed and regenerated O_2 and PO_4^{3-} concentrations were calculated with a data-constrained ocean circulation model. The model has a horizontal resolution of 2° with 24 vertical levels, and assimilates temperature, salinity, radiocarbon and CFC-11 observations to obtain a climatological steady-state ocean circulation that is consistent with both the tracer data and dynamical constraints[15,16]. Preformed O_2 and PO_4^{3-} (collectively, tracer) concentrations are calculated by dividing the ocean into a surface region above the compensation depth, z_c, and an interior region below z_c. In the surface region the tracers are set to their observed values from interpolating the 2009 World Ocean Atlas[17,18] objectively mapped tracer concentrations to the model grid. The World Ocean Atlas data are available at http://www.nodc.noaa.gov/OC5/WOA09/pr_woa09.html. In the interior region, preformed tracer concentrations are calculated by assuming that the only source or sink of tracer is physical transport from the surface region by ocean currents and mixing processes. Regenerated tracer concentrations are then calculated by subtracting the calculated preformed concentrations from observed total tracer concentrations. This method of calculating regenerated oxygen concentrations (equivalent to the negative of the True Oxygen Utilization, or TOU (ref. 29)) implicitly takes into account oxygen undersaturation in the surface ocean, thereby avoiding known biases incurred when using apparent oxygen utilization (AOU) to estimate oxygen consumption[29]. The ratio of regenerated oxygen to regenerated phosphate is then calculated at each interior ocean grid point,

$$R_{O_2:P}(\mathbf{r_I}) = -\frac{O_{2,reg}(\mathbf{r_I})}{PO_{4,reg}{}^{3-}(\mathbf{r_I})} \quad (1)$$

where $\mathbf{r_I}$ is the set of interior ocean grid points. We exclude model grid points in the Arctic Ocean and Mediterranean Sea from our analysis, owing to insufficient observational constraints on the circulation in these regions. We also exclude from our analysis several grid points where regenerated O_2 and PO_4^{3-} concentrations fall below a certain threshold, and are therefore considered unreliable (see Supplementary Methods for details). These exclusions do not affect our results or conclusions.

An ensemble of simulations was carried out by repeating the calculations with a range of z_c from 36 m to 114 m, corresponding to the top three model layers; with 11 different configurations of the data-constrained circulation model which vary in aspects such as the depth of the surface mixed layer and the values of sub-gridscale diffusivities; and with both annually averaged and winter-averaged observations of both O_2 and PO_4^{3-} from the 2009 World Ocean Atlas. These combinations yield 66 different simulations of the preformed and regenerated O_2 and PO_4^{3-} concentrations in the interior ocean (11 different circulation models ×3 different compensation depths ×2 different O_2 and PO_4^{3-} fields). These 66 different simulations are used to derive uncertainty estimates for all values calculated here.

For dividing the surface ocean into distinct biomes based on light and nutrient availability (Fig. 2a), a chlorophyll-weighted annually averaged solar radiation dose (SRD) climatology was computed using SeaWIFS satellite data, following the procedure described in the Supplementary Methods. Surface solar irradiance data is available at data.giss.nasa.gov/seawifs/ and chlorophyll concentrations can be found at oceancolor.gsfc.nasa.gov. Surface nitrate concentrations were taken from the 2009 World Ocean Atlas.

O_2 concentrations predicted under uniform stoichiometric conditions (Fig. 3) were calculated by multiplying the estimated regenerated PO_4^{3-} concentrations by the volume-averaged global $R_{O_2:P}$ value from each model simulation to obtain a 'uniform $R_{O_2:P}$-predicted' regenerated O_2 concentration. Volume-averaged global $R_{O_2:P}$ values vary between 127 and 167 in our suite of model simulations, with a mean value of 147 (Supplementary Table 1). The uniform $R_{O_2:P}$-predicted regenerated O_2 concentration was then added to the estimated preformed O_2 from each model simulation, to obtain the O_2 concentration predicted under uniform O_2:P stoichiometry. The effects of denitrification were taken into account in these calculations by correcting the regenerated PO_4^{3-} concentrations using previously estimated denitrification rates[30] and standard denitrification stoichiometry[10,21]. Accounting for denitrification increases the global mean $R_{O_2:P}$ value by approximately three to five units.

Received 30 May 2014; accepted 22 October 2014; published online 24 November 2014

References

1. Arrigo, K. R. *et al.* Phytoplankton community structure and the drawdown of nutrients and CO_2 in the Southern Ocean. *Science* **283,** 365–367 (1999).
2. Green, S. E. & Sambrotto, R. N. Plankton community structure and export of C, N, P, and Si in the Antarctic Circumpolar Current. *Deep-Sea Res. II* **53,** 620–643 (2006).
3. Weber, T. & Deutsch, C. Ocean nutrient ratios governed by phytoplankton biogeography. *Nature* **467,** 550–554 (2010).
4. Martiny, A. C. *et al.* Strong latitudinal patterns in the elemental ratios of marine plankton and organic matter. *Nature Geosci.* **6,** 279–283 (2013).
5. Martiny, A. C., Vrugt, J. A., Primeau, F. W. & Lomas, M. W. Regional variation in the particulate organic carbon to nitrogen ratio in the surface ocean. *Glob. Biogeochem. Cycles* **27,** 723–731 (2013).
6. Karl, D. M. *et al.* Ecological nitrogen-to-phosphorus stoichiometry at Station ALOHA. *Deep-Sea Res. II* **48,** 1529–1566 (2001).
7. Ito, T. & Follows, M. Preformed phosphate, soft tissue pump and atmospheric CO_2. *J. Mar. Res.* **63,** 813–839 (2005).
8. Lenton, T. M. & Watson, A. J. Redfield revisited: 1. Regulation of nitrate, phosphate, and oxygen in the ocean. *Glob. Biogeochem. Cycles* **14,** 225–248 (2000).
9. Redfield, A. C., Ketchum, B. H. & Richards, F. A. in *The Sea* Vol. 2 (ed. Hill, M.) Ch. 2, 26–77 (Interscience, 1963).
10. Paulmier, A., Kriest, I. & Oschlies, A. Stoichiometries of remineralisation and denitrification in global biogeochemical ocean models. *Biogeosciences* **6,** 923–935 (2009).
11. Weber, T. & Deutsch, C. Ocean nitrogen reservoir regulated by plankton diversity and ocean circulation. *Nature* **489,** 419–422 (2012).
12. Takahashi, T., Broecker, W. S. & Langer, S. Redfield ratio based on chemical data from isopycnal surfaces. *J. Geophys. Res.* **90,** 6907–6924 (1985).
13. Anderson, L. A. & Sarmiento, J. L. Redfield ratios of remineralization determined by nutrient data analysis. *Glob. Biogeochem. Cycles* **8,** 65–80 (1994).
14. Körtzinger, A., Hedges, J. I. & Quay, P. D. Redfield ratios revisited: Removing the biasing effect of anthropogenic CO_2. *Limnol. Oceanogr.* **46,** 964–970 (2001).
15. DeVries, T. & Primeau, F. Dynamically and observationally constrained estimates of water-mass distributions and ages in the global ocean. *J. Phys. Oceanogr.* **41,** 2381–2401 (2011).
16. DeVries, T. The oceanic anthropogenic CO_2 sink: Storage, air-sea fluxes, and transports over the industrial era. *Glob. Biogechem. Cycles* **28,** 631–647 (2014).
17. Garcia, H. E. *et al.* in *World Ocean Atlas 2009* Vol. 4 (ed. Levitus, S.) 398 (US Government Printing Office, 2010).
18. Garcia, H. E. *et al.* in *World Ocean Atlas 2009* Vol. 3 (ed. Levitus, S.) 344 (US Government Printing Office, 2010).
19. Bianchi, D., Dunne, J. P., Sarmiento, J. L. & Galbraith, E. D. Data-based estimates of suboxia, denitrification, and N_2O production in the ocean and their sensitivities to dissolved O_2. *Glob. Biogeochem. Cycles* **26,** GB2009 (2012).
20. Geider, R. & LaRoche, J. Redfield revisited: Variability of C:N:P in marine microalgae and its biochemical basis. *Eur. J. Phycol.* **37,** 1–17 (2002).

21. Anderson, L. A. On the hydrogen and oxygen content of marine phytoplankton. *Deep-Sea Res. I* **42,** 1675–1680 (1995).
22. Hopkinson, C. S. & Vallino, J. J. Efficient export of carbon to the deep ocean through dissolved organic matter. *Nature* **433,** 142–145 (2005).
23. Pahlow, M. & Oschlies, A. Chain model of phytoplankton P, N, and light colimitation. *Mar. Ecol. Prog. Ser.* **376,** 69–83 (2009).
24. Toseland, A. *et al.* The impact of temperature on marine phytoplankton resource allocation and metabolism. *Nature Clim. Change* **3,** 979–984 (2013).
25. Dickman, E. M., Vanni, M. J. & Horgan, M. J. Interactive effects of light and nutrients on phytoplankton stoichiometry. *Oecologia* **149,** 676–689 (2006).
26. Bopp, L. *et al.* Multiple stressors of ocean ecosystems in the 21st century: Projections with CMIP5 models. *Biogeosciences* **10,** 6225–6245 (2013).
27. Sarmiento, J. L., Hughes, T. M. C., Stouffer, R. J. & Manabe, S. Simulated response of the ocean carbon cycle to anthropogenic climate warming. *Nature* **393,** 245–249 (1998).
28. Friedlingstein, P. *et al.* Climate-carbon cycle feedback analysis: Results from the C^4MIP model intercomparison. *J. Clim.* **19,** 3337–3353 (2006).
29. Ito, T., Follows, M. J. & Boyle, E. A. Is AOU a good measure of respiration in the oceans? *Geophys. Res. Lett.* **31,** L17305 (2004).
30. DeVries, T., Deutsch, C., Rafter, P. A. & Primeau, F. Marine denitrification rates determined from a global 3-D inverse model. *Biogeoscience* **10,** 2481–2496 (2013).

Acknowledgements

This research was supported by a grant from the US National Science Foundation (OCE-1131548) and by the Gordon and Betty Moore Foundation (grant GBMF3775).

Author contributions

T.D. performed the model calculations. Both authors designed the study, analysed the data and wrote the paper.

Additional information

Supplementary information is available in the online version of the paper. Reprints and permissions information is available online at www.nature.com/reprints. Correspondence and requests for materials should be addressed to T.D.

Competing financial interests

The authors declare no competing financial interests.